Simulation of HF Circuits with FDTD Technique Including Non-Ideal Lumped Elements

P. Ciampolini, P. Mezzanotte, L. Roselli, D. Sereni, R. Sorrentino, P. Torti

Istituto di Elettronica, Università di Perugia
S. Lucia Canetola, I-06131 Perugia, Italy

Abstract

An extension of the FDTD algorithm is devised, accounting for high-frequency models of lumped elements. Bipolar transistors, junction and Schottky diodes are considered, as well as their associated non linear capacitances. Several validation examples are given. In particular, a simple, yet complete, structure has been simulated, consisting of an L-band unbalanced mixer and including a microstrip stub, a microstrip to microstrip TEE junction, a microstrip gap and a shielding package. Results favourably compare with alternative simulation techniques.

1. Introduction

The FDTD technique has been widely adopted for the numerical solution of Maxwell's equation over complex domains [1,2,3]. More recently, extended formulations of such an algorithm have been worked out [4,5], that account for lumped elements. This makes FDTD suitable for the simulation of circuits including semiconductor active devices (such as diodes and bipolar transistors). In order to properly account for the inherently nonlinear behavior of these devices, however, some algorithmic complexities are to be faced: for this reason, only fairly simple device models have been considered up to now. Most notably, only low-frequency, large-signal equivalent circuits have been taken into account.

In this abstract, we describe the inclusion of a more general set of models into our 3D-FDTD Maxwell's equation solver: more specifically, the conventional, low-frequency models have been incorporated into the code, and supplemented with equations modeling the non-linear, intrinsic capacitances associated with pn junctions and metal-semiconductor junctions.

The resulting discretization scheme is summarized in Section 2 below, whereas some simulation results are described in Section 3. In particular, some elementary structures have been simulated to validate the method and illustrate its features. The simulation of a more realistic structure, i.e., an unbalanced mixer with a filtering stub, is also discussed. Finally, conclusions are drawn in Section 4.

2. Models of lumped elements

To account for lumped elements, it is convenient to split the conduction current $\overline{J}_c$, appearing in the Maxwell's curl $\overline{H}$ equation:

$$curl(\overline{H}) = \varepsilon \frac{d\overline{E}}{dt} + \overline{J}_c \quad , \tag{1}$$

into two separate contributions:

$$\overline{J}_c = \overline{J}_{cd} + \overline{J}_{cl}. \tag{2}$$

Here, $\overline{J}_{cd}$ represents the contribution of the current flowing along the distributed media (expressed the customary way within the FDTD scheme), whereas $\overline{J}_{cl}$ stands for the contribution of the lumped element(s). For a simple pn-junction diode, the lumped-element current can be expressed as follows:

$$I = I_d + I_c = I_d + \frac{dQ_d}{dt} = I_s\left(e^{q\frac{V_d}{kT}} - 1\right) + C_d(V_d)\frac{dV_d}{dt} \tag{3}$$

In the above equation, the capacitance *Cd(Vd)* is determined by two concurrent effects, namely the width modulation of the space-charge region and the injection of minority carriers across the junction; consequently, two terms [6, 7] are accounted for :

$$C_d(V_d) = C_J + C_D \tag{4}$$

where C_j is the junction capacitance, given by:

$$C_J(V_d) = C_J(0)\cdot\left(1 - \frac{V_d}{\Phi_0}\right)^{-m} \quad \text{if } V_d < F_c \cdot \Phi_0 \tag{5a}$$

$$C_J(V_d) = \frac{C_J(0)}{F_2}\cdot\left(F_3 + \frac{m\cdot V_d}{\Phi_0}\right) \text{ if } V_d \geq F_c \cdot \Phi_0 \tag{5b}$$

In Eqs. (5), m is a coefficient related to the doping profile (m=0.5 for abrupt junction), Φ_0 is the junction built-in voltage and F_C,F_2, F_3 are suitable constants. In Eq. (5b) a regional approximation is assumed: the forward bias capacitance of Eq. (5b) comes from a linear extrapolation of the expression (5a), valid within the reverse bias region. In forward-bias regimes, however, the dynamic behavior is largely dominated by the diffusion capacitance below:

CH3577-4/95/0000-0361$01.00 © 1995 IEEE

$$C_D = \frac{q}{KT}\tau_D I_s\left(e^{\frac{q}{K\cdot T}\cdot V_d} - 1\right) \qquad (6)$$

in which τ_d represents the lifetime of minority carriers. Schottky diodes are modeled in the same way, except for the absence of the diffusion capacitance. Bipolar transistors are taken into account by arranging a network of non-ideal junction diodes and current-controlled current-sources, according to the scheme depicted in Fig. 1b [6].

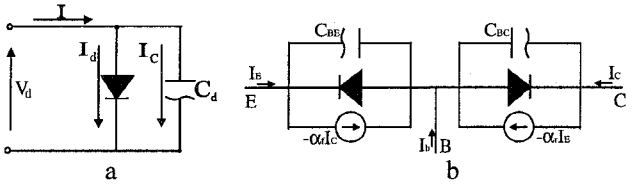

Figure 1: Diode (a) and bipolar transistor (b) equivalent circuits.

For the sake of conciseness, we shall focus the following discussion on the junction-diode model. Accounting for Eqs. (3) through (6), and assuming the standard Yee notation, the discretization of the lumped-element current density appearing in (1) can be carried out. Following the same approach of Sui at al. [4], we find, for the x-component:

$V_D \geq -F_c \cdot \Phi_0$:

$$J_{clx}^{n+\frac{1}{2}}(i+\tfrac{1}{2},j,k) = -\frac{I_0}{\Delta y\cdot\Delta z}\cdot\left(e^{-\frac{q}{K\cdot T}\Delta x\frac{E_x^{n+1}(i+\frac{1}{2},j,k)+E_x^n(i+\frac{1}{2},j,k)}{2}} - 1\right) + \frac{1}{\Delta y\cdot\Delta z}\cdot\left\{\tau_D\cdot I_0\cdot\frac{q}{K\cdot T}\cdot e^{-\frac{q}{K\cdot T}\Delta x\frac{E_x^{n+1}(i+\frac{1}{2},j,k)+E_x^n(i+\frac{1}{2},j,k)}{2}} + C_J(0)\cdot\left[1+\frac{\Delta x}{\Phi_0}\cdot\frac{(E_x^{n+1}(1+\frac{1}{2},j,k)+E_x^n(1+\frac{1}{2},j,k))}{2}\right]^{-m}\right\}\cdot \Delta x\cdot\frac{E_x^{n+1}(1+\frac{1}{2},j,k)-E_x^n(1+\frac{1}{2},j,k)}{\Delta t}$$

$V_D < F_c \cdot \Phi_0$:

$$J_{clx}^{n+\frac{1}{2}}(i+\tfrac{1}{2},j,k) = -\frac{I_0}{\Delta y\cdot\Delta z}\cdot\left(e^{-\frac{q}{K\cdot T}\Delta x\frac{E_x^{n+1}(i+\frac{1}{2},j,k)+E_x^n(i+\frac{1}{2},j,k)}{2}} - 1\right) + \frac{1}{\Delta y\cdot\Delta z}\cdot\left\{\tau_D\cdot I_0\cdot\frac{q}{K\cdot T}\cdot e^{-\frac{q}{K\cdot T}\Delta x\frac{E_x^{n+1}(i+\frac{1}{2},j,k)+E_x^n(i+\frac{1}{2},j,k)}{2}} + \frac{C_J(0)}{F_2}\cdot\left[F_3 - \frac{m\cdot\Delta x}{\Phi_0}\cdot\frac{(E_x^{n+1}(1+\frac{1}{2},j,k)+E_x^n(1+\frac{1}{2},j,k))}{2}\right]\right\}\cdot \Delta x\cdot\frac{E_x^{n+1}(1+\frac{1}{2},j,k)-E_x^n(1+\frac{1}{2},j,k)}{\Delta t} \qquad (7b).$$

Unlike Sui et al.[4], time derivatives in Eq. (7) are actually averaged between time-steps n and $n+1$; this ensures consistency with the discretization adopted for remaining terms in Eq. (1). By incorporating Eq. (7), the discretized expression of Eq. (1) becomes strongly non-linear. A damped Newton-Raphson procedure is used to iteratively seek for the solution. In order to avoid divergence of such a loop, it is often necessary to reduce the simulation time step well below the constraint imposed by the Courant stability criterion. Hence, although non-linearities usually affect only a negligible fraction of the equations to be solved, the computational effort required by the simulation may significantly increase due to the inclusion of non-linear lumped elements. Some strategies to reduce such an overhead are currently being investigated.

3. Results

The first structure we have simulated consists of a simple clamping diode placed across an ideal, parallel-plate waveguide: the FDTD simulation results are shown in Fig. 2(a), which compares the current predicted by the ideal (dashed line) and non-ideal (solid line) diode models. The input waveguide signal is a 1 GHz, null-offset sinewave: the non-ideal response significantly deviates from the ideal one, mostly due to the diode turn-off transient.

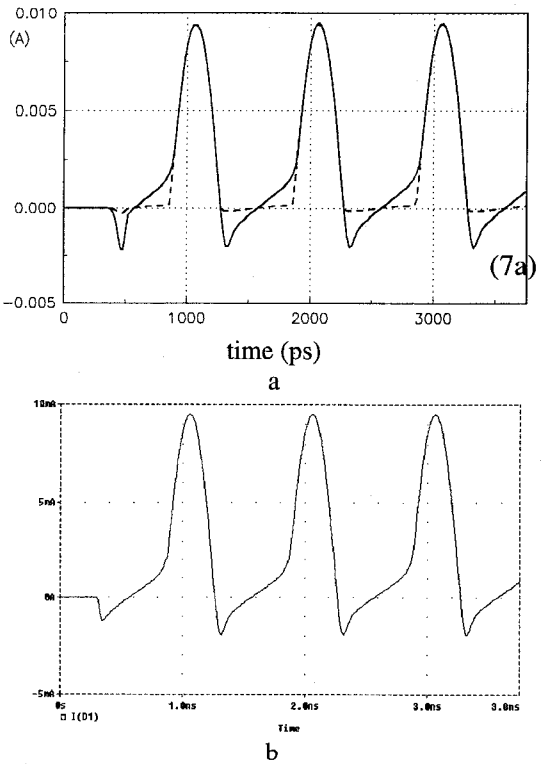

Figure 2: Comparison between FDTD (a) and SPICE (b) simulation results.

A further comparison is given in Fig. 2(b), where SPICE simulation results for a similar structure are found: the simple case at hand easily lends itself to the equivalent circuit representation needed by SPICE, so that an excellent agreement between the two results is found.

Fig. 3 illustrates the influence of intrinsic capacitances over the small-signal behavior of a common emitter BJT amplifier: the plot refers to predicted computed currents for a 2 GHz input signal. The result makes it evident a transconductance loss, mainly due to C_{be}.

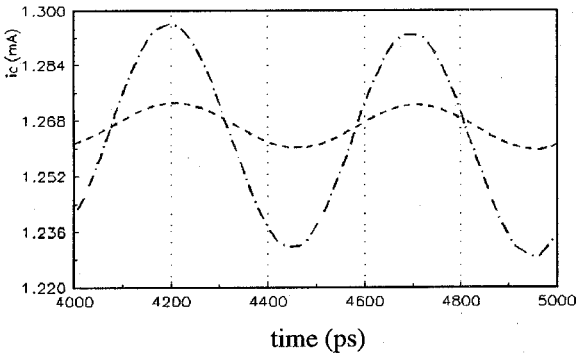

Figure 3: Output current of a CE amplifier. Ideal (dot-dashed line) and non ideal (dashed line) models.

A more realistic application is shown in Fig. 4 and consists of a unbalanced mixer, based on a Schottky diode series-connected to a filtering microstrip stub. The line is terminated by a load resistor, connected to the ground plane through a via-hole, while the simulation domain is bound by the metallic package.

The transient response of the FDTD simulation is shown in Fig. 5(a), together with the extracted frequency spectrum (Fig. 5(b)). Such results are in fair agreement with those of Figs. 6, predicted by the harmonic balance technique adopted by HP-MDS. Small, quantitative discrepancies between Figs. 5 and 6 are to be ascribed to the different models adopted for the passive network: in particular, the full wave technique exploited by FDTD accounts for a more comprehensive physical picture of the structure of Fig. 4.

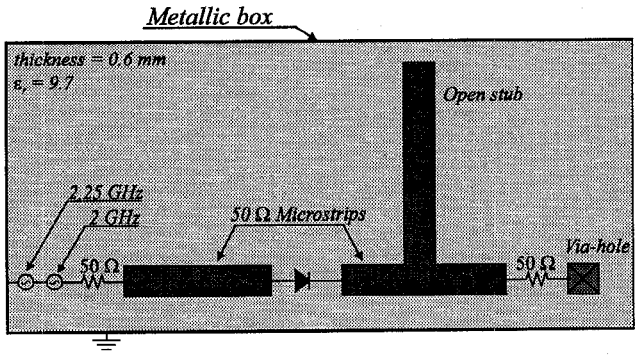

Figure 4: layout of the simulated circuit.

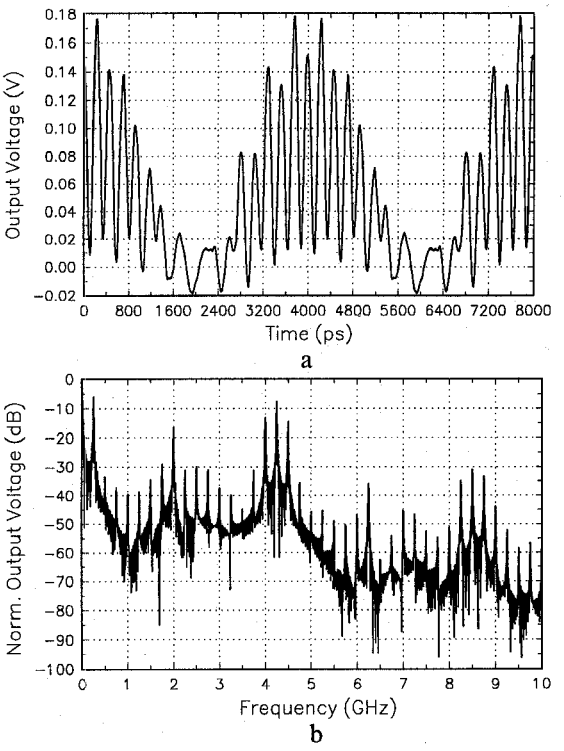

Figure 5: mixer output voltage (a) and frequency spectrum (b) as computed by FDTD.

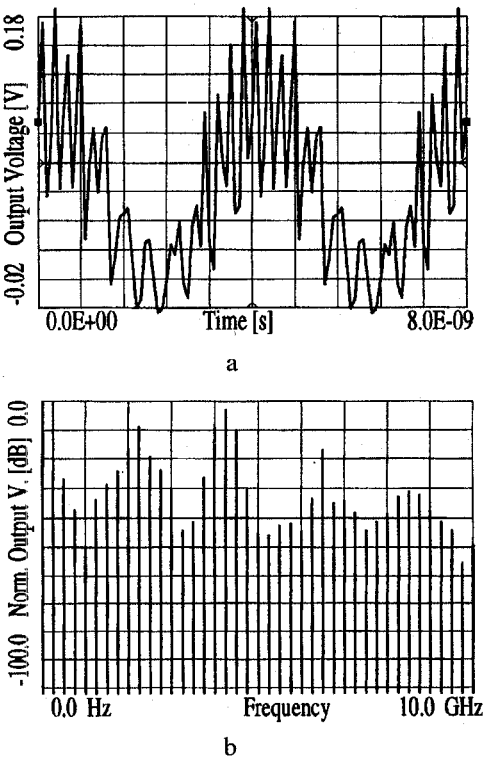

Figure 6: mixer output voltage (a) and frequency spectrum (b) as computed by HP- MDS.

4. Conclusions

An extension of the FDTD algorithm has been proposed, aimed at making it suitable for the simulation of circuits operating at high frequencies and including non-ideal, non-linear lumped elements. Models of the non linear capacitances associated to pn junctions have been discretized consistently with the leapfrog algorithm adopted for the solution of Maxwell's equations.

The code features models of bipolar and Schottky junction diodes and BJTs, as well as lumped resistances, capacitors and inductors, independent voltage sources and controlled current sources. These elements, in turn, can be regarded as elementary building blocks, suitable for future assembling of large-signal models of further kinds of lumped elements (e.g., field effect transistors).

A few simulation examples have been discussed to validate the algorithm. The more demanding simulation of an unbalanced microwave mixer has been carried out, providing reliable results and thus demonstrating the effectiveness of the lumped-elements FDTD technique as a high-frequency circuit-analysis tool.

References

[1] K. S. Yee, "Numerical Solution of Initial Boundary Value Problems Involving Maxwell's Equations in Isotropic Media," IEEE Trans. AP, vol. AP-14, pp. 302-307, May 1966.

[2] A. Taflove and M. E. Brodwin, "Numerical Solution of Steady-State Electromagnetic Scattering Problems Using the Time-Dependent Maxwell's Equations," IEEE Trans. MTT, vol. MTT-23, pp. 623-630, Aug. 1975.

[3] M. Rittweger and I. Wolff, "Analysis of Complex Passive (M)MIC Components Using the Finite Difference Time-Domain Approach," 1990 Intl. IEEE MTT-S Digest, pp. 1147-1150.

[4] W. Sui, D. A. Christensen and C. H. Durney, "Extending the two-dimensional FD-TD method to hybrid electromagnetic systems with active and passive lumped elements", IEEE Trans. MTT, vol. MTT-40, pp. 724-730, Apr. 1992.

[5] M. Piket-May, A.Taflove and J. Baron, "FD-TD Modeling of Digital Signal Propagation in 3-D circuits with Passive and Active Loads", IEEE Trans. MTT, vol. MTT-42, pp. 1514-1523, Aug. 1994.

[6] S. M. Sze, "Physics of Semiconductor Devices", John Wiley

[7] G. Massobrio, P. Antognetti, "Semiconductor Device Modeling with SPICE 2/E", McGraw-Hill.